J Ind Microbiol Biotechnol (2013) 40:1161–1180
DOI 10.1007/s10295-013-1308-0

SYSTEMS BIOTECHNOLOGY

Genome-scale stoichiometry analysis to elucidate the innate capability of the cyanobacterium *Synechocystis* for electricity generation

Longfei Mao · Wynand S. Verwoerd

Received: 13 May 2013 / Accepted: 20 June 2013 / Published online: 14 July 2013

Abstract *Synechocystis* sp. PCC 6803 has been considered as a promising biocatalyst for electricity generation in recent microbial fuel cell research. However, the innate maximum current production potential and underlying metabolic pathways supporting the high current output are still unknown. This is mainly due to the fact that the high-current production cell phenotype results from the interaction among hundreds of reactions in the metabolism and it is impossible for reductionist methods to characterize the pathway selection in such a metabolic state. In this study, we employed computational metabolic techniques, flux balance analysis, and flux variability analysis, to exploit the maximum current outputs of *Synechocystis* sp. PCC 6803, in five electron transfer cases, namely, ferredoxin- and plastoquinol-dependent electron transfers under photoautotrophic cultivation, and NADH-dependent mediated electron transfer under photoautotrophic, heterotrophic, and mixotrophic conditions. In these five modes, the maximum current outputs were computed as 0.198, 0.7918, 0.198, 0.4652, and 0.4424 A gDW^{-1}, respectively. Comparison of the five operational modes suggests that plastoquinol-/c-type cytochrome-targeted electricity generation had an advantage of liberating the highest current output achievable for *Synechocystis* sp. PCC 6803. On the other hand, the analysis indicates that the currency metabolite, NADH-, dependent electricity generation can rely on a number of reactions from different pathways, and is thus more robust against environmental perturbations.

Keywords Microbial fuel cell (MFC) · *Synechocystis* sp. PCC 6803 · Bioelectricity · Flux balance analysis · Flux variability analysis

Introduction

Synechocystis sp. PCC 6803 has become a popular model photosynthetic organism studied by many researchers after its genome was fully sequenced in the 1990s [15, 33]. Since this cyanobacteria species is a photoautotroph that divides rapidly, it has been enlisted as a platform for production of biofuels by using sunlight as an inexpensive energy source [1, 14]. However, biofuels need to be further processed (e.g., combustion) to be transformed into a usable energy form such as electricity. An alternative way to exploit the energy production potential of *Synechocystis* sp. PCC6803 is to apply this prokaryote as biocatalyst in a microbial fuel cell (MFC), so as to directly convert metabolic activity inside the cell into electricity.

Synechocystis sp. PCC6803 in MFCs can produce current through three mechanisms: mediated electron transfer (MET) [47, 57, 67], direct electron transfer (DET) [26, 31], and product modes (reviewed in [28]). For the product mode, hydrogen produced by *Synechocystis* sp. PCC 6803 can be in situ oxidized at the anode, releasing the electrons to the electric circuit. Akin to the green algae *C. reinhardtii*, *Synechocystis* sp. PCC 6803 relies on hydrogenases for hydrogen generation [9]. However, these enzymes are 100 times less active than the analogues of *C. reinhardtii*

Electronic supplementary material The online version of this article (doi:10.1007/s10295-013-1308-0) contains supplementary material, which is available to authorized users.

L. Mao (✉) · W. S. Verwoerd
Centre for Advanced Computational Solutions,
Department of Molecular Biosciences, Lincoln University,
Ellesmere Junction Road, Lincoln 7647, New Zealand
e-mail: longfei.mao@lincolnuni.ac.nz

W. S. Verwoerd
e-mail: wynand.verwoerd@lincoln.ac.nz

[20] and their activities can be inactivated by O_2. This creates a major barrier for practical hydrogen production. Moreover, the anodic oxidation of hydrogen demands a high pressure that causes safety issues. Due to these biochemical and engineering limitations, it would be impractical to further study the use of *Synechocystis* sp. PCC 6803 in product-mode current production.

In the DET mode, the cytochromes of the electron transfer chain in the cell membrane can directly release electrons to the anode. This operation mode requires attachment of the cell to the anode. Unlike another exoelectrogen, *G. sulfurreducens*, in which the electrons are derived from biochemical oxidation of organic compounds via the respiratory electron transfer chain [25], *Synechocystis* sp. PCC 6803 has an advantage that it obviates the need of exogenous organic fuel and thus its electrogenic activities are entirely dependent on the energy of light [41, 42, 72]. In the DET mode, *Synechocystis* sp. PCC6803 achieved a steady power density of 6.7 mW m^{-3} (peaking at 7.5 mW m^{-3}) [26, 31]. This power density is still much lower than the values achieved by other commonly used biocatalysts. Nevertheless, because the DET mode of this cyanobacterium is directly linked to its photosynthetic activity and the quoted measurement is quite recent, it is worth exploring if this organism has the potential to deliver competitive power densities.

For the MET mode, an exogenous mediator is involved as an electron relay to pull the elections away from metabolism and deliver them to a remote electron acceptor (anode) [49]. *Synechocystis* sp. PCC 6803 are prokaryotes, and their simpler cell membranes and internal structure are more amenable to physical electron extraction than eukaryotes. Two intracellular redox carriers, reduced ferredoxin and plastoquinol, have been proposed to be the electron sources targeted by mediators such as 2-hydroxy-1,4-nepthoplastoquinol (HNQ) [47, 57, 67] in MFCs.

In addition to these two shuttles, the currency molecule NADH has received considerable attention [8, 16, 43, 47, 64, 69]. NADH is universally involved in the energy metabolism of all living organisms. Maintaining a proper balance of NAD^+/NADH is a primary biological objective that is important to biomass production [58]. Any steps of NADH regeneration in the intracellular electron-transfer pathways in cells could be targeted by exogenous mediators, such as Bromocresol Green (BG) and neutral red (NR), which can convey the electrons to an extracellular electrode (anode) [2, 32, 38]. Importantly, due to the relatively low (negative) potential of NADH, it has been proposed that the theoretical limit of MFC voltage output is the potential difference between NADH and the reaction in the cathode in an MFC [23, 43]. Therefore, targeting NADH as the electron source in MFCs of MET mode can liberate the maximum power achievable for a microorganism.

Since *Synechocystis* sp. PCC6803 has been actively studied as a promising biocatalyst for electricity generation in this study, we employed computational metabolic engineering tools to elucidate the innate current capability of *Synechocystis* sp. PCC6803 for current production. Specifically, (1) we performed flux balance analysis (FBA) to compute the maximum amperage output and pertinent metabolic behaviors of *Synechocystis* PCC6803 in the five electron transfer cases consisting of (Table 1): ferredoxin- and quinone-dependent photoautotrophic mode, NADH-dependent photoautotrophic, heterotrophic, and mixotrophic modes; Recently, FBA has been successfully used to study another microorganism, *Shewanella oneidensis* MR-1 (a commonly used MFC biocatalyst), for metabolic behaviors under different growth conditions [11, 40, 53]; (2) We then investigated the trade-offs between amperage output and the biomass production (growth) rate; (3) For elucidation of the fundamental metabolic mechanisms supporting the desired electron transfer in the five cases, we implemented flux variability analysis (FVA), to compute the strategies used by the cell to maximize the current production, subject to stoichiometric balance and substrate uptake; (4) In the end, we analyzed the effect of varying substrate (i.e., the glucose and photon) uptake rate on the growth rate and the amperage output in the each of the five modes.

Materials and methods

General modeling assumptions

The assumptions used for the present modeling were described in a previous study [30] of the prokaryote

Table 1 The metabolism and electron transfer types investigated in the present metabolic modeling

Organisms	Transfer type	Electron source (terminal bacterial electron shuttle)	Metabolic type	
Synechocystis sp. PCC6803	Membrane-driven	Ferredoxin	Aerobic	Photoautotrophic
		Plastoquinol/c-type cytochrome (*)		Photoautotrophic
	Mediator-driven	NADH		Photoautotrophic
				Heterotrophic
				Mixotrophic

* The flux model of *Synechocystis* cannot identify the difference between these two sites for electricity generation

Geobacter sulfurreducens. In general, the system that is modeled satisfies three conditions: (1) The MFC reactor is a chemostat that can provide optimum conditions to meet all the needs of microbial growth; (2) Only a pure *Synechocystis* sp. PCC 6803 culture is used for electricity generation and (3) For the MET mode, a putative ideal mediator (e.g., Neutral red [37]) is added that can enter cytoplasm and transfer electrons from the reduced ferredoxin, plastoquinol, or NAD^+/NADH cycle to the anode; (4) The c-type cytochrome in the electron transfer chain is the electron source for the DET mode (as schematically detailed in Fig. 1).

Although the MFC electricity generation based on the DET mode of the *Synechocystis* has been experimentally observed [41, 42], the molecular mechanisms (what proteins and what reactions) underlying the DET has not been clearly elucidated for this strain (albeit it is proposed that the electron transfer chain in the membrane related to the electrogenic activity). Therefore, to examine the current production potential of the DET mode of the *Synechocystis* in the present modeling, an assumption is made based on the general paradigm of the mechanisms of the DET mode—the c-type chromosome-mediated electron transfer. Such a DET mechanism has been well established for the two most commonly used MFC biocatalysts, *Geobacter* sp. and *Shewanella* sp. (reviewed by [28]). These two species possess nanowires, electrically conductive bacterial appendages, to directly transport electrons from cells to solid electron acceptors such as graphite anodes in MFCs [13, 44, 45] and this electron transfer process is fundamentally mediated by the c-type cytochrome in the cell membrane [4, 35]. Since these two microbes and the *Synechocystis* are all Gram-negative prokaryotes sharing similar cell membrane structures, the present study presumed that the state-of-the-art DET mechanism in the *Synechocystis* would be mediated by the c-type cytochromes.

Modeling electrode interactions

The interactions with an electrode were captured by introducing six reactions into the model reconstruction (Table 2).

When the electricity generation is linked to the reduced ferredoxin, electrons are deprived of this redox shuttle, accompanied by accumulation of oxidized ferredoxin. Thus, we model this process by introducing the equation: ferredoxin → ferredoxin_mfc. As is clear from the stoichiometry in Table 7, each reduced ferredoxin as used in the model carries only one electron, which is different from NADH.

The efficiency of the DET mode is dependent on the availability of type-c cytochrome. The production of this cytochrome is catalyzed by cytochrome b_6f complex (plastoquinol—cytochrome-*c* reductase) through the reaction (EC: 1.10.2.2): plastoquinol + 2 ferricytochrome c → plastoquinone + 2 ferrocytochrome c. The reaction indicates that the plastoquinol acts as an intrinsic mediator that can reduce the c-type cytochrome [19]. Since the c-type cytochrome production reaction is not included in the original model, it was subsequently added and served as another objective for the FBA modeling. However, from a modeling perspective, it was found that maximization of the flux through this added reaction makes no difference from maximization of plastoquinol available for MFC. This means the plastoquinol-dependent MET mode and the cytochrome c-based DET mode have the same current output potentials.

These added reactions (Table 2) denote the net reaction between the reducing equivalents and the electrodes in MFCs, with mediators not shown because they act as intermediates only. Introduction of these reactions creates an additional escape channel for electrons, and their fluxes are subject to the mass balance rule in the FBA modeling. Since the reactants (i.e., ferredoxin, plastoquinol, and NADH) of these reactions are native metabolites of the microorganisms, the added equations do not cause production of non-native by-products. These processes are schematically detailed in Fig. 1. NADPH is not expected to be an efficient feedstock for external current production and is not considered further here.

Because this study aimed at elucidation of the electricity generation potential of this microorganism, we only modeled the function of mediators and left room for other ongoing research to identify or engineer an ideal mediator, as reviewed in [18, 50, 52, 55, 66], which is suitable for practical extraction of the electrons from the redox metabolites in different configurations of MFCs based on *Synechocystis* sp. PCC 6803.

Objective equation

The objective equation was formulated as described in our recent study [29], and only the method outline is presented here.

The metabolic states of the bio-catalytic cells in MFCs are governed by two objectives, one is for survival, represented as maximization of biomass production in the FBA modeling, the other one is production of a surplus reducing equivalent flux sustaining electric current, which can be mathematically described as maximization of conversion of low energetic oxidized redox equivalents (e.g., NAD^+) to their highly energetic counterparts (e.g., NADH). The two objectives could compete with each other and thus a trade-off optimization between the two can form a Pareto front, comprising a set of Pareto-optimal points [39]. Every Pareto-optimal point is equivalent to the

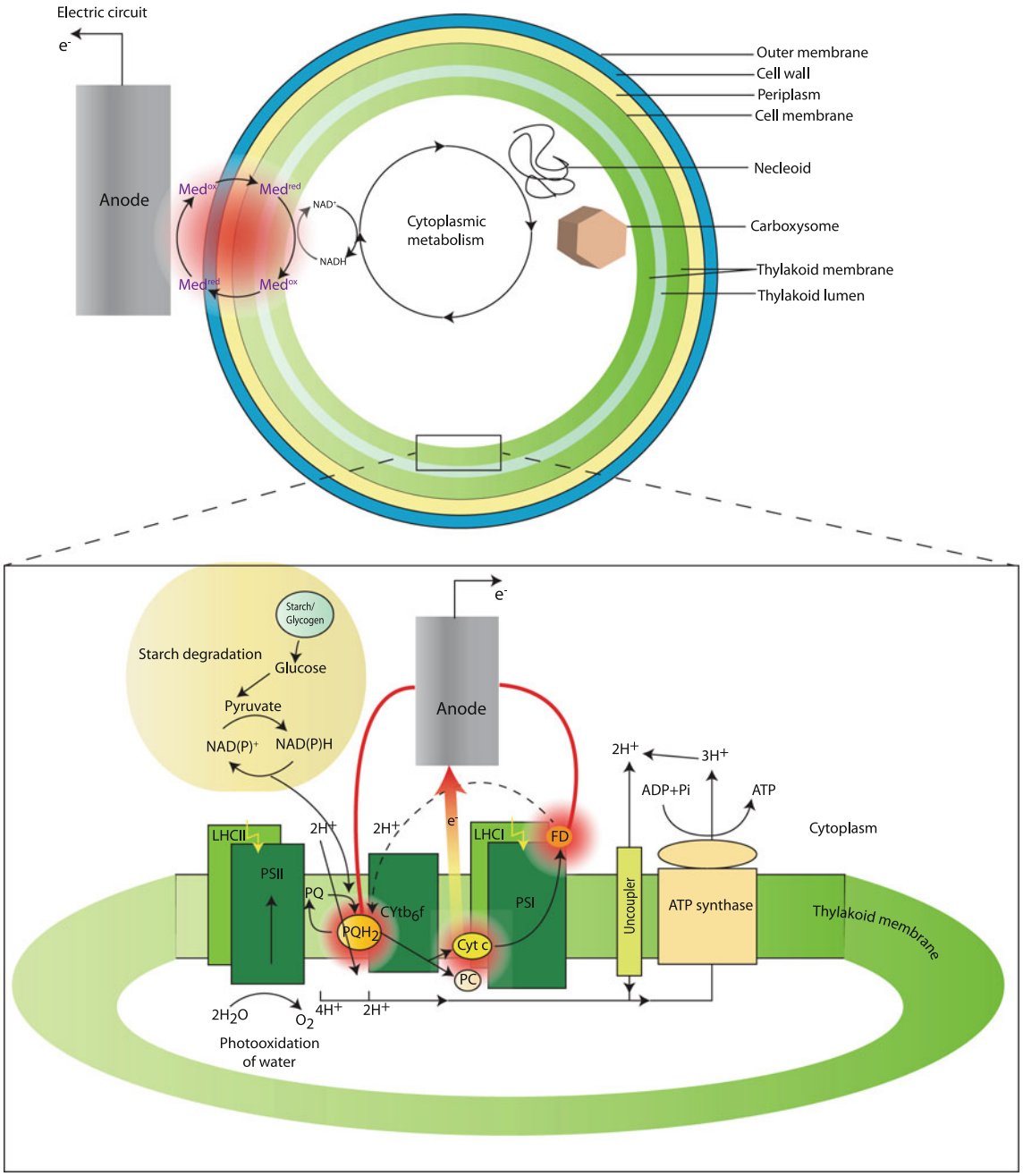

Fig. 1 The anodic mechanisms of *Synechocystis* sp. PCC 6803 modeled in the present study. The electron transfers are established between an electrode and three potential intracellular electron shuttles: (1) ferredoxin and (2) plastoquinol pool (MET) or type-c cytochromes (DET) in the photosynthetic and respiratory transfer chain, and (3) NADH in the cytoplasmic metabolism in *Synechocystis* sp. PCC6803. Microbes take up substrates (i.e., glucose and/or light) generating carbon dioxide and protons. This process yields electrons for metabolic benefit, i.e., growth, and reduces Med_{ox} in the cytosol into Med_{red}. Med_{red} diffuses into contact with the electrode, where Med_{red} reduces the electrode generating electrical current. The oxidized form, Med_{ox}, diffuses back through the anolyte for reuse by the microbes. The *insert* is a schematic representation of the intersecting photosynthetic and respiratory electron transport pathways in thylakoid membranes of *Synechocystis* sp. PCC 6803. Photosynthesis takes place in a thylakoid membrane and mainly involves two membrane-spanning protein complexes, namely Photosystem 1 (PS1) and Photosystem 2 (PS2). These two complexes are interconnected by a number of enzymes and co-factors, forming a photosynthetic electron transfer chain along which proton-motive gradient is generated across the thylakoid membrane for ATP production. The *red thick line* indicates the putative electron transfer path between the pETC and the electrode, and the *radial red circle* highlights the site supplying electrons towards the electrode. Thylakoids are vase-shaped, and occur in pairs. *PQ* plastoquinone, *PQH2* plastoquinol, *PC* plastocyanin, *Cyt c* C-type cytochrome, *PS I* photosystem I, *PS II* photosystem II, *LHC I* light harvesting complex I, *LHC II* light harvesting complex II (color figure online)

Table 2 The added reactions for modeling the interaction of the microorganisms and the electrode in MFCs

Operation mode of the MFC	Reaction ID	Reaction
Ferredoxin-dependent MET	ferred_mfc	ferred → ferred_mfc
	EX_ferred_mfc	ferred_mfc → feroxd
Plastoquinol-dependent MET/cytochrome *c* dependent DET	qh2_mfc	qh2 → qh2_mfc
	EX_qh2_mfc	qh2_mfc → q
NADH-dependent MET	1NADHmfc	nadh → nadh_mfc
	2NADHmfc	nadh_mfc → nad + h_emm

Other abbreviations are detailed in [70]

ferred_mfc the reduced form of ferredoxin that supply the electrons to anode, *qh2_mfc* the plastoquinol that supply electrons to anode, *nadh_mfc* the NADH available for MET mode of MFCs, *h_emm* the H ions as the by-product released from the Reaction 2NADHmfc

solution of a weighted-sum optimization with a different (unspecified) set of weights [10]. Varying the relative weights associated with individual objectives allows us to evaluate the impact of the enhanced current extraction on cellular metabolism. This is represented in our study by defining the objective as follows in terms of the biomass growth flux F_B and the reducing equivalent diversion flux F_N:

$$o = (1 - \lambda) F_B + \lambda g F_N$$

A unit conversion factor g is explicitly provided because in the model, F_N and F_B are measured respectively in units mmol/gDW/h and g/gDW/h or (h^{-1}). This ensures that λ is a dimensionless fraction that can be directly interpreted as the relative contribution of the NADH flux to the combined objective.

Fractional benefit analysis

The bi-objective optimization implemented in the present study represents that the cell intends to survive a continuous metabolic energy loss during current production. The use of an objective function is a mathematical method to evaluate how current production influences growth, but it cannot elucidate the combined benefit resulting from an optimized metabolic state. This is demonstrated by considering either extreme on the Pareto front; even though only one of the objective terms is maximized, the other term also has a value and will contribute (positively or negatively) to the overall benefit.

In order to mathematically quantify this, we scale each of F_B and F_N as a fraction of the maximal values F_B^* and F_N^* they can ever achieve, i.e., the values when each is independently maximized. As the maximum of each of these fractions is 1, a plausible measure of the combined benefit achieved in any particular metabolic state is the value of the quantity we denote as the fractional benefit B:

$$B = \frac{1}{2}\left(\frac{F_N}{F_N^*} + \frac{F_N}{F_N^*}\right)$$

This measure was used in Fig. 3 to highlight the way that different growth conditions produce different responses in terms of combining cell growth and external current yield. A value of B in excess of 50 %, indicates that gains in one objective more than compensates for losses in the competing objective.

Simulating the growth of *Synechocystis* sp. PCC6803

Synechocystis sp. PCC 6803 grow photoautotrophically on light, heterotrophically on glucose, or mixotrophically on both light and glucose. For the mixotrophic condition, glucose uptake rate was set to 0.38 mmol gDW^{-1} h^{-1}, which was experimentally obtained [68]. The effective photon uptake rate was set to 15.4 mmol gDW^{-1} h^{-1} (0.889 μE m^{-2} s^{-1}), because this photon uptake rate results in the experimentally obtained flux value of the reaction catalyzed by RuBisCO when the glucose uptake rate was set to the experimentally obtained one (0.38 mmol gDW^{-1} h^{-1}) [68, 70] and illuminated by one circular cool white 32-W fluorescent lamp (the a light intensity of 125 μmol m^{-2} s^{-1}) [68]. For heterotrophic growth, the maximum glucose uptake rate is constrained to an experimentally measured value, 0.85 mmol gDW^{-1} h^{-1} [68], and photon uptake rate was set to zero. Besides, the following external metabolites were allowed to freely transport through the cell membrane: CO_2, H_2O, SO_3, NO_3, and PO_4. Nitrate was assumed as sole nitrogen source, and ammonium uptake rate was set to zero for all simulations [70]. For autotrophic growth, glucose uptake rate was set to zero and the photon uptake rate was set to the given value same as for mixotrophic growth.

Photon uptake rate

In contrast to previous studies [51, 70], in which the whole cell surface area was assumed to intercept photon flux during illumination, this study considered the cross section of the exposed orientation of the cell to determine the incident photon flux.

Dimensional photon flux conversion factor

The dry mass of a typical *Synechocystis* cell is taken to be 0.5 pg [22] and the diameter of the *Synechocystis* cell is assumed to be 1.75 μm [21] with a spherical geometry. Based on the same assumption as discussed for *C. reinhardtii*, the cross-sectional area of *Synechocystis* is calculated to be 2.405 μm^2. With these values, the unit of the photon uptake rate (μE m^{-2} s^{-1}) can be converted into the rate of reaction flux (mmol gDW^{-1} h^{-1}) in the modeling as follows:

$$1\ \mu E\ m^{-2}\ s^{-1} = \frac{1\ \mu E}{m^2\ s} \times \frac{2.405\ \mu m^2}{0.5\ pg} \times \frac{pg}{10^{-12}\ g} \times \frac{10^{-12}\ m^2}{\mu m^2} \times \frac{3,600\ s}{h} \times \frac{1\ mE}{1,000\ \mu E} = 17.316\ mE\ gDW^{-1}\ h^{-1}$$

$$\text{Conversion}_{\text{Dim}} = \frac{17.316\ mE/gDW/h}{1\ \mu E/m^2/s}$$

Effective photon flux conversion factor

$$\text{Conversion}_{\text{Eff}} = \frac{15.4\ mE/gDW/h}{125\ \mu E/m^2/s\ \times \text{Conversion}_{\text{Dim}}} = 0.007115\ \text{effective/incident photon flux}$$

This model indicated an effective photon flux conversion factor of 0.007115 for *Synechocystis* sp. PCC6803, which means 0.7115 % of incident photons are absorbed metabolically by the cell. This value is lower than the 3.75 % calculated for *C. reinhardtii* [5].

Conversion of units of flux and current

Current (in amperes) was integrated over time and converted to electrons recovered by using the following conversions: 1 C = 1 A × 1 s, 1 C = 6.24 × 10^{18} electrons, and 1 mol = 6.02 × 10^{23} electrons (Faraday's constant 96485 C/mol). Therefore, one flux unit (mmol/g/h) can be converted into A/g as follows:

$$1\ \text{mmol/g/h} = \frac{1\ \text{mol}}{1,000\ \text{g} \times 3,600\ \text{s}} \times \frac{96,485\ \text{C}}{\text{mol}} = 0.0268\ \text{A/g}$$

Coulombic efficiency (CE)

One of the parameters commonly used to quantify the performance of MFCs is coulombic efficiency (CE). The CE is defined as the ratio of electrons transferred to the anode to that in the starting substrate. We use the full oxidation of glucose with oxygen as the oxidant as the reference reaction to characterize the energy efficiency of the respiratory metabolism:

Glucose oxidation reaction: $C_6H_{12}O_6 + 6\ H_2O \rightarrow 6\ CO_2 + 24\ H^+ + 24\ e^-$

Based on such stoichiometric information, 1 mol of glucose supplies 24 mol of electrons [17].

$$\text{CE}\,\% = \frac{C_{\text{output}}}{C_{\text{substrate}}} \times 100\,\% = \frac{\text{The MET flux(mmol/gDW/h)} \times 100}{\text{acetate uptake rate (mmol/gDW/h)}\ \times 24}\ \%$$

The metabolic efficiency of converting photons into external MFC current can be calculated based on the stoichiometries of the photon-involved reaction in the network model below (Table 3). Each absorbed photon liberates two electrons since each qh_2 (plastoquinol) carries two electrons [6].

Thus, the coulombic efficiency can be calculated using the formula as follows:

$$\text{CE}\,\% = \frac{C_{\text{output}}}{C_{\text{substrate}}} \times 100\,\% = \frac{\text{The MET flux(mmol/gDW/h)} \times 100}{\text{photon uptake rate (mmol/gDW/h)}\ \times 2}\ \%$$

Calculation of theoretical power outputs of the five tested modes

An upper limit for the cell voltage is calculated in this work based on formal potentials (at pH 7) of the biological and electrochemical redox processes, as given by:

$$\Delta E^{\circ'}_{\text{cell}} = E^{\circ'}_{\text{cathode}} - E^{\circ'}_{\text{anode}}$$

where $\Delta E^{\circ'}_{\text{cell}}$ is the standard cell potential (aka., electromotive force); $E^{\circ'}_{\text{cathode}}$is the standard potential of cathode oxidation; $E^{\circ'}_{\text{anode}}$ is the standard potential of anode reduction. The formal potentials of the anode and cathode used for calculation of power density in the five operation modes are summarized in Table 4.

The actual potential derived from the MFC will be lower due to various potential losses [24] associated with MFC operation, such as ohmic resistances, concentration polarization, and kinetic constraints. These are not taken into account in the calculations reported here.

The MFC standard cell potential calculated as above and shown in Table 5 shows that as long as the same electron

Table 3 List of two light-dependent reactions in the network model [70]

Photosynthesis and electron transport chain	2 h2o + 4 photon + 4 q + 8 H → 4 H[t] + O2 + 4 qh2
	4 qh2 + 2 nadp + 2 H + 4 photon → 4 q + 2 nadph + 8 H[t]

The abbreviations of the metabolites are listed in [70]

Table 4 The standard potential of the anodic and catholic reactions funneling electrons to the electrode, measured at pH 7, versus standard hydrogen electrode (SHE)

	Redox couple	$E^{\circ'}$(V)
Anode		
MET	Ferredoxin(Fe^{3+}) + $e^- \rightarrow$ Ferredoxin(Fe^{2+})	−0.420 [43]
	$NAD^+ + H^+ + 2e^- \rightarrow NADH$	−0.320 [63]
	Ubiquinone + $2H^+$ + $2e^- \rightarrow$ Ubiquinone H_2	+0.100 [63]
DET	Cytochrome *c* (Fe^{3+}) + $e^- \rightarrow$ Cytochrome *c* (Fe^{2+})	+0.254 [63]
Cathode	$O_2 + 4H^+ + 4e^- \rightarrow 2H_2O$	+0.51 [7, 49, 71]

Table 5 The theoretical limit of standard anode potentials of MFC

Electron transfer mode	$E^{\circ'}_{anode}$	$E^{\circ'}_{cathode}$	$\Delta E^{\circ'}_{cell}$
MET	−0.32	0.51	0.83
DET	0.254	0.51	0.256

donors are used, the choice of microbe will have little effect on the cell potential.

Analysis technique

In this study we chose a recent metabolic network of *Synechocystis* sp. 6803, reconstructed by a research group from Osaka University, as the backbone for all in silico analyses [70]. It is noted that another metabolic network of *Synechocystis* sp. 6803 (iJN678), published in the same period but by a different research group from the University of Iceland, was also available. The two network models were not compared with each other by the authors. For this study, we used the Osaka model, because (1) this version was verified not only by the experimental data but also through comparison of prediction capabilities with several previous landmark metabolic networks of *Synechocystis* sp. PCC6803 [54, 70]; (2) This model received more attention by experts in this field (discussed in a review article) [54]; (3) it was free of inadequate reaction loops. Furthermore, the Osaka model contains about 41 % fewer reactions than iJN678, but considers nearly threefold more genes of the cyanobacterium. Since the two models are both at genome scale, further statistical evidence may be needed to assess the predictive ability of the two models.

The original network model in Excel format was parsed into SBML using the converter integrated in the NetSplitter [61, 62]. The SBML file of the model is supplied (Additional file 1). The growth rates and electron production were computationally determined using FBA [36, 59]. Computations were performed with COBRA Toolbox [48] in MATLAB (The Math-Works Inc., Natick, MA, USA) and OptFlux [46]. Flux variability analysis (FVA) [27] was conducted to determine the flux ranges of the reactions in the network under the metabolic states heavily perturbed by electricity generation and can be performed with either COBRA or OptFlux according to users' preference. The maximum reducing equivalent production rates for arbitrary growth rates between the data points were calculated using the interpolation function in Mathematica 8.0 (Wolfram Research, Inc. Champaign, IL, USA). All the FBA and FVA results are detailed in the Additional file 2.

Results and discussion

Impact of the redox perturbation on the biomass production

Figure 2 shows that the production of MFC current competes with biomass production for metabolic resources. In the metabolic state of optimal growth, all redox flux was consumed for maximizing the biomass production rate. As the oxidized forms of the reducing metabolites (i.e., reduced ferredoxin, plastoquinol, and NADH) were converted into their oxidized counterparts due to the deprivation of electrons by mediators for current production, the metabolic resources for biomass growth were diverted towards reducing equivalent generation so as to restore a proper redox balance for maintaining a viable growth state. In all five modeled electron transfer cases, the rise in current production was accompanied by a continuous drop in growth rates. When the current production rates approached their maximum allowable values, the corresponding biomass formation rates were suppressed to near their minimum values. This indicates that a large portion of energy is converted into electricity and the remaining metabolic resource is only sufficient for a low growth rate.

Comparison of the regeneration rates of the desired reducing equivalents at optimal growth states and highly perturbed current-producing states (Table 6) shows that the *Synechocystis* could elevate the plastoquinol regeneration rate more readily than for reduced ferredoxin and NADH. This implies that the metabolism of the cyanobacterium is naturally more tolerant to disturbance of a plastoquinol leak than stress situations resulting from ferredoxin and NADH perturbation, when light is the sole feedstock. It is found that, compared with the optimal growth state, the cell had a capability to increase the total ferredoxin regeneration rate by about 179.4 fold (17,839 %), achieving a total reduced ferredoxin flux of 7.567 mmol/gDW/h. This indicates that ferredoxin flux level is not compulsory to survival (growth) of *Synechocystis,* but it is allowed to

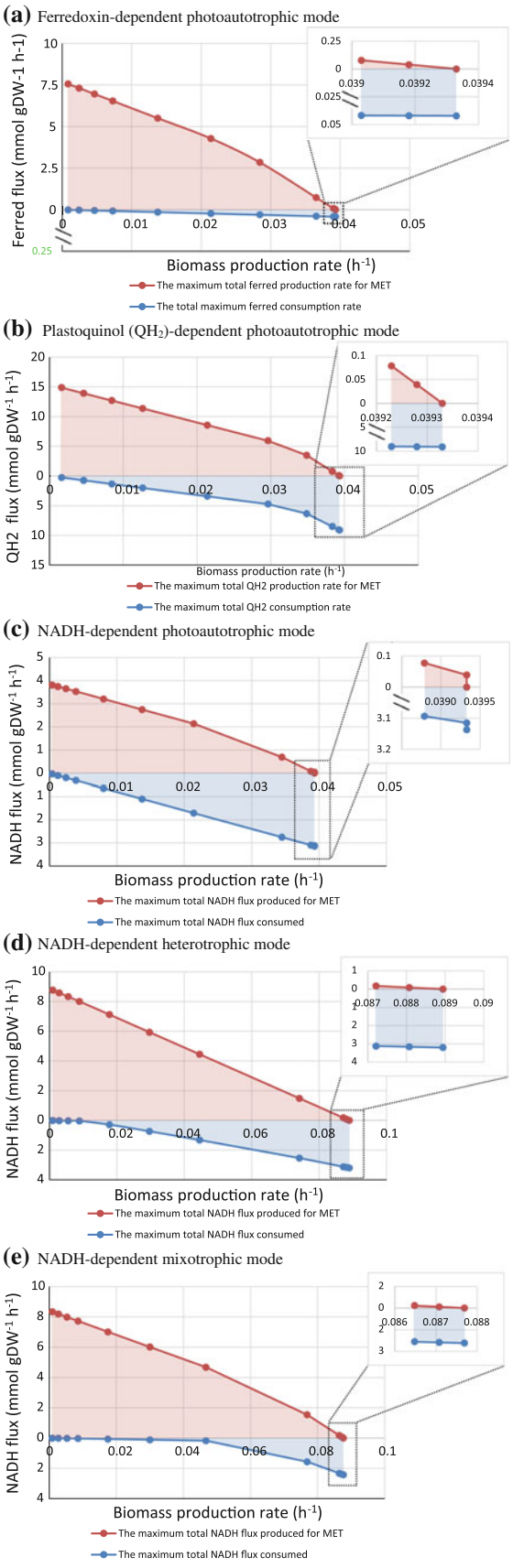

◀ **Fig. 2** Relationships of the biomass production and electron transfer rates. The production rate of external MFC current carriers and the reducing equivalent consumption rate for cellular use, as functions of biomass production rate. The *red line* represents the maximal reducing equivalent supplying rate for a feasible biomass production rate, while any point within the *pink* area represents all allowable reducing equivalent supplying rates and biomass production rates. The *blue* area represents the total reducing equivalent consuming flux for normal cellular function. The distance between the two lines across the *pink* and *blue* areas represents the total available reducing equivalent flux in the cell at a metabolic state related to a specific biomass production rate; inset, enlargement of *boxed* area. The reducing equivalent denotes reduced ferredoxin, plastoquinol, or NADH in respective cases above. QH_2 reduced plastoquinol, *ferred* reduced ferredoxin. The points are simulated by bi-objective optimization involving varying coefficients (λ) assigned for the growth and MET maximizations. A more detailed discussion of the significance of the λ is given in the "Materials and methods" section. Briefly, it is a parameter that continuously adjusts the metabolic state of the cell through a range stretching from pure growth without the extraction of current (at one extreme) to at state in which all metabolic resources are taken up by supplying electric current and no growth, at the other extreme (color figure online)

up-regulate to eliminate uncontrolled adverse conditions, such as an overoxidized state caused by electron deprivation of the reduced ferredoxin. In addition, *Synechocystis* achieved the highest NADH turnover rate in the heterotrophic mode, followed by the mixotrophic mode, and the lowest in the photoautotrophic mode. This is due to the highest substrate uptake rates set for the heterotrophic mode among the three nutritional modes.

The present modeling limited the substrate uptake rate to a realistic range (see "Materials and methods" section) to maximize the objectives and allow the metabolism to freely adjust. Nevertheless, in all simulations of the heterotrophic and mixotrophic modes, the glucose uptake rates were at the maximum bounds (0.85 mmol/gDW/h for the heterotrophic and 0.38 mmol/gDW/h for the mixotrophic conditions). This indicates that the enhanced reducing equivalent regeneration, as presented in Fig. 2, is mainly associated with the reallocation of metabolic resource from growth towards the desired electron shunt.

The MFC current production rates shown in the top parts of Fig. 2 for the five cases show a linear dependence on biomass growth for small growth rates and only deviates slightly from that for larger growth rates. The relationships between varying biomass production rate and the electron transfer rate appears simpler than that found in our recent work on the eukaryote *C. reinhardtii* [29] and which was characterized by different growth types and current production modes. For that organism, starting from the unperturbed state of zero MET production at the right-hand side of the plots, a type I behavior was described as the increase in the current production rate without any change the biomass production rate; in Fig. 2, only a single point

Table 6 Increases in the desired redox metabolite production rate at metabolic states optimized for current production compared with their control states optimized for growth

Operational mode	Control state (mmol/gDW/h)	Maximum current production state (mmol/gDW/h)	Fold change	Increase (%)
Ferredoxin-targeted photoautotrophic	0.04218	7.567	179.4	17,839
QH_2-targeted photoautotrophic	9.114	15.14	1.661	66
NADH-targeted photoautotrophic	3.137	3.850	1.227	23
NADH-targeted heterotrophic	3.200	8.779	2.743	174
NADH-targeted mixotrophic	2.426	8.339	3.437	244

for the NADH-targeted photoautotrophic mode displays evidence of type I behavior. This behavior demonstrates reallocation of metabolic resources without compromising growth and should repress some possible functional phenotypes, i.e., number of alternative optimal solutions, at the optimal growth rate.

Type II behavior, where the curvature of the current-carrier curve shows that the yield obtained when sacrificing biomass growth progressively decreases, is most pronounced for the QH_2-dependent photoautotrophic mode, less visible for the other cases that involve photosynthesis, and totally absent in heterotrophic growth. This behavior is interpreted as a loss of conversion efficiency, as a higher current demand reduces the feasibility to satisfy this demand by metabolic pathways with high efficiency but comparatively low capacity.

Finally, the linear (type III) behavior observed for heterotrophic growth and all other modes at high current demands, shows that when only a small number of pathways remain with the required capacity to supply these demands, efficiency ceases to play a role, and there is a straightforward trade-off between biomass growth and current production.

Further support for this interpretation comes from a more detailed comparison of the individual reactions that participate in supplying reducing equivalent, as presented in the "Metabolic strategies" section below. For example, in the heterotrophic mode, lack of light input suppresses the photophosphorylation and cascading reactions. The linear correlation between the MFC current production and biomass growth indicates that the remaining reactions associated with electricity production possessed the same efficiency in NADH regeneration. Therefore, there are no slope alteration stages in the electron diversion curve resulting from the switch between the high-efficiency and the high-capability reactions.

The behavior of the NADH consumption for maintenance (Fig. 2) is also much simpler for *Synechocystis* than for *C. reinhardtii*. Again, curved and linear relationships to the growth rates are observed for similar reasons as discussed above for the external current production. However, for *C. Reinhardtii* [29], all metabolic conditions showed a range of growth rates where the NADH consumption increases with a decrease of growth rate, but for *Synechocystis*, the NADH consumption monotonically decreases as the growth rate decreases in all five cases shown in Fig. 2.

Taken together, the differences from the complex interrelations between MFC current production and the reducing equivalent consumption behaviors in the cases of *Chlamydomonas reinhardtii* [29] indicates that the closer correspondence for *Synechocystis* reflects the simpler prokaryotic metabolism. Since the linear dependence on biomass production was found for the whole heterotrophic curve but present in only part of the curves for the photoautotrophic and mixotrophic modes, it is indicated that the photoautotrophic and mixotrophic metabolic characteristic of *Synechocystis* sp. PCC6803 were similar, which is in accordance with a previous study [56].

The discussion above suggests a general competition between the reducing equivalent shunt and biomass production in all five cases. To further elucidate the change in the metabolic efficiency as the electron shunt augments, we introduce a measure called the fractional benefit B, as discussed in the "Materials and methods" section, to quantify the metabolic optimality regarding the network output in the form of both biomass and reducing equivalent production rates.

Figure 3 shows the result of this measure applied to the reported simulations. Starting from wild-type growth rates (right-hand side of the figures), the B values generally increased to reach an apex, the best metabolic state for the dual objectives, and then decreased since the further improvement in reducing equivalent generation rate was at a high cost of biomass production rate. This behavior was easily distinguishable in the photoautotrophic and mixotrophic cases, but not in the heterotrophic mode. The highest combined benefit (near 58 %) was achieved with the plastoquinol-targeted photoautotrophic mode. This indicates that plastoquinol-linked MET or the c-type cytochrome targeted DET mode are the most suitable intracellular electron resource for current production. However, this B value (near 58 %) is still lower than the lowest maximum values for the NADH-dependent MET

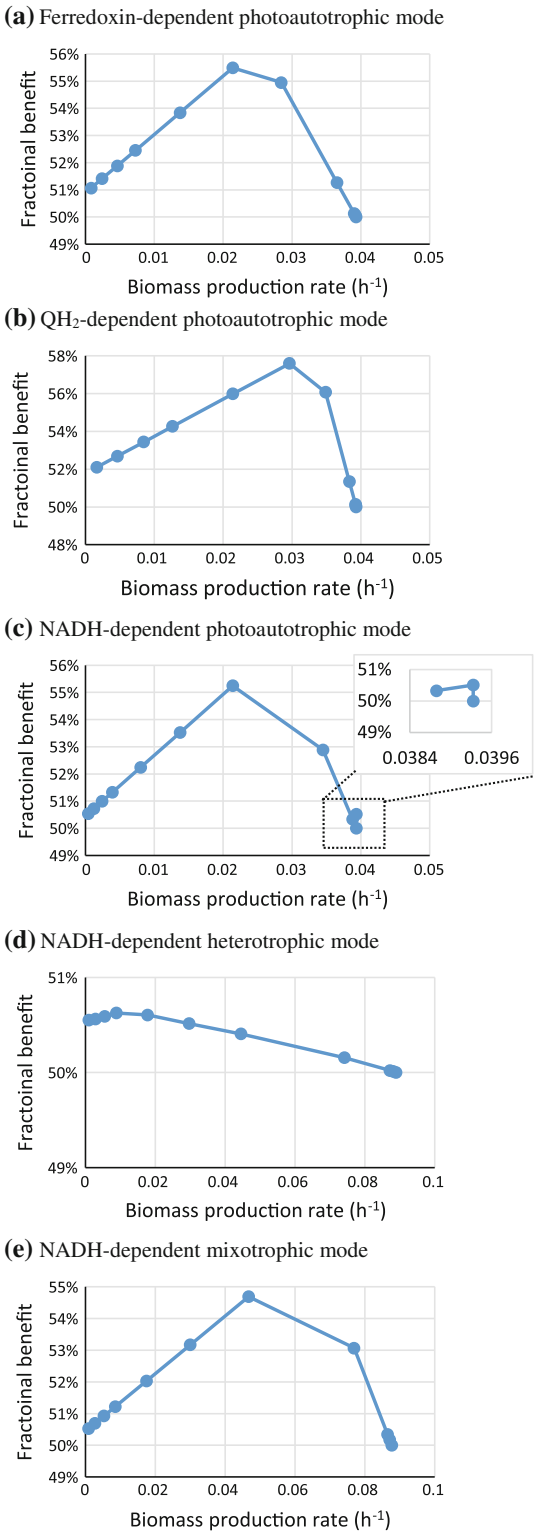

Fig. 3 Effect of varying biomass production on the fractional benefit. The fractional benefit B plotted on the vertical axis is a measure of success in achieving the combined goals of maximal growth rate and MET flux. Maximizing one of these at a time, as at the endpoints, gives only B = 50 %. The graphs show that relative to this, gains in MET flux can more than offset losses of growth rate in the *Synechocystis* sp. PCC 6803 metabolism

mode of *C. reinhardtii* in all three cultivations (i.e., hetero-, photoauto-, and mixotrophic). This could imply that *Synechocystis* is less resilient to redox perturbation than *C. reinhardtii*, a eukaryote. The lowest maximum fractional benefit was found in the case of the heterotrophic mode, where the B values resulted from all the simulations could not even reach 51 %. This suggests that there is a strong competition between the biomass production and the NADH-dependent current production when glucose is the sole metabolic fuel. The peak shown in the insert of Fig. 3c corresponds to the enlargement in Fig. 2c, and indicates that a small NADH shunt is tolerable to the photoautotrophic growth and thus can improve the metabolic optimality defined here (i.e., fractional benefit B value).

The metabolic mechanisms underlying the high reducing equivalent regeneration rates in the aforementioned electron transfer cases are elucidated in the next section. Tables 7, 8, 9, 10, and 11 summarize a list of reactions (enzymes) that were chosen by the cell to promote the diversion of the reducing fluxes towards current production.

Metabolic strategies for sustaining a high flux of reducing equivalents in the five electron transfer cases

For elucidation of the enzymatic mechanisms underlying the high current production in the three modes, we chose metabolic states modeled with λ of 0.9998 as the reference state for the maximum current production because a further increase in λ can barely increase the electron transfer rates when the λ was above 0.999. In fact, for identifying the metabolic behaviors under high electron transfer rates, any λ above 0.999 can produce an extremely perturbed metabolic state, since they all represent the metabolic states at which nearly all metabolic resources have been relocated from for biomass production to the current production.

Ferredoxin (ferred)-dependent photoautotrophic mode

When the mediator deprives reduced ferredoxin of electrons forming oxidized counterparts, the oxidized/reduced ferredoxin ratio in the metabolism is disturbed and consequently the cell has to adjust its metabolic pathways to restore a proper redox balance in order to survive.

Table 7 shows six reactions in the metabolism of *Synechocystis* sp. PCC 6803 involving ferredoxin production, but only one reaction, catalyzed by ferredoxin-NADP oxidoreductase (EC: 1.18.1.2), was found to be responsible for the identified maximum output ferredoxin flux (7.310 mmol/gDW/h) for current production. This reaction had a capability to regenerate reduced ferredoxin at rates ranging from 7.313 to 11.49 mmol/gDW/h, which could

Table 7 The identified reactions that contribute significantly to the predicted maximum current output in the ferredoxin-dependent photoautotrophic mode

Reaction ID	Ferredoxin (mmol/gDW/h)		Enzyme	EC no.	Reaction	Subsystem
	Min	Max				
133	−4.176	0	Ferredoxin-dependent glutamate synthase	EC:1.4.7.1	gln-L + akg + 2 ferred → 2 glu-L + 2 feroxd	Glutamate, glutamine biosynthesis
138	0	0	Nitrate reductase	EC:1.7.7.2	Nitrate + 2 ferred → nitrite + h2o + 2 feroxd	Glutamate, glutamine biosynthesis
139	0	0	Ferredoxin-nitrite reductase	EC:1.7.7.1	Nitrite + 6 ferred + 6 H → nh3 + 2 h2o + 6 feroxd	Glutamate, glutamine biosynthesis
149	−0.00264	−0.00264	Sulfite reductase	EC:1.8.7.1	h2s + 6 feroxd + 3 h2o ⟺ SO3 + 6 ferred + 6 H	Glycine, serine, cysteine biosynthesis
169	0	0	Pyruvate oxidoreductase	EC:1.2.7.1	Feroxd + pyr + coa → ferred + accoa + co2	Glycolysis
279	7.313	11.49	Ferredoxin-NADP oxidoreductase	EC:1.18.1.2	2 ferred + nadp + H ⟺ 2 feroxd + nadph	Photosynthesis and electron transport chain

Reaction ID and metabolite abbreviations are detailed in [70]

Table 8 The identified reactions that contribute significantly to the predicted maximum current output in the plastoquinol-dependent photoautotrophic mode

Reaction ID	QH_2 flux (mmol/gDW/h)		Enzyme	EC no.	Reaction	Subsystem
	Min	Max				
280	0	0	N/A	N/A	2 H + 0.5 O2 + qh2 → 2 H[t] + h2o + q	Photosynthesis and electron transport chain
281	14.66		N/A	N/A	2 h2o + 4 photon + 4 q + 8 H → 4 H[t] + O2 + 4 qh2	Photosynthesis and electron transport chain
284	−0.7414	−0.7414	N/A	N/A	4 qh2 + 2 nadp + 2 H + 4 photon → 4 q + 2 nadph + 8 H[t]	Photosynthesis and electron transport chain
285	−0.00007	−0.00007	N/A	N/A	fadh2 + q ⟺ fad + qh2	Photosynthesis and electron transport chain
286	0	0	NADH dehydrogenase	EC:1.6.99.3,1.6.5.3	nadh + 5 H + q → 4 H[t] + nad + qh2	Photosynthesis and electron transport chain
287	0	0	NADH dehydrogenase	EC:1.6.99.3,1.6.5.3	nadph + 5 H + q → 4 H[t] + nadp + qh2	Photosynthesis and electron transport chain

Reaction ID and metabolite abbreviations are detailed in [70]

N/A not available

Table 9 The identified reactions that contribute significantly to the predicted maximum current output in the NADH-dependent photoautotrophic mode

Reaction ID	NADH_mfc (mmol/gDW/h)		Enzyme	EC no.	Reaction	Subsystem
	Min	Max				
73	0	7.779	NAD(P) transhydrogenase	EC:1.6.1.2	nadph + nad → nadp + nadh	Energy metabolism
106	−0.0005	7.778	Enoyl-ACP reductase	EC:1.3.1.9	dodecaACP + nad ⟺ tddec2eACP + nadh + H	Fatty acid biosynthesis
140	0.00114	3.890	D-3-phosphoglycerate dehydrogenase	EC:1.1.1.95	3 pg + nad ⟺ 3ppop + nadh + H	Glycine, serine, cysteine biosynthesis
171	−2.722	7.684	Glyceraldehyde-3-phosphate dehydrogenase	EC:1.2.1.59	gap + pi + nad ⟺ bpg + nadh + H	Glycolysis
251	−0.00051	7.778	Homoserine dehydrogenase	EC:1.1.1.3	hom-L + nad ⟺ aspsa + nadh + H	Methionine biosynthesis
288	0	3.889	delta-1-pyrroline-5-carboxylate dehydrogenase	EC:1.5.1.12 1.5.99.8	1pyr5c + nad + 2 h2o → glu-L + nadh + H	Proline biosynthesis
NADH consuming reactions						
134	−3.941	0	Glutamate synthase	EC:1.4.1.14	gln-L + akg + nadh + H → 2 glu-L + nad	Glutamate, glutamine biosynthesis
381	−3.940	0.00101	2-ketoacid dehydrogenase malate dehydrogenase lactate dehydrogenase	EC:1.1.1.37	mal + nad ⟺ oaa + nadh + H	TCA cycle

See Additional file 2 for the FVA results of all 32 reactions involving NADH; Reaction ID and metabolite abbreviations are detailed in [70]

Table 10 The identified reactions that contribute significantly to the predicted maximum current output in the NADH-dependent heterotrophic mode

Reaction ID	NADH flux (mmol/gDW/h)		Enzyme	EC	Reaction	Subsystems
	Min	Max				
73	0	3.021	NAD(P) transhydrogenase	EC:1.6.1.2	nadph + nad → nadp + nadh	Energy metabolism
106	−0.00115	3.020	Enoyl-ACP reductase	EC:1.3.1.9	dodecaACP + nad ⟺ tddec2eACP + nadh + H	Fatty acid biosynthesis
171	1.410	4.431	Glyceraldehyde-3-phosphate dehydrogenase	EC:1.2.1.59	gap + pi + nad ⟺ bpg + nadh + H	Glycolysis
251	−0.00117	3.020	Homoserine dehydrogenase	EC:1.1.1.3	hom-L + nad ⟺ aspsa + nadh + H	Methionine biosynthesis
377	2.772	2.772	Dihydrolipoamide dehydrogenase	EC:1.8.1.4	dlipo + nad ⟺ lipo + nadh + H	TCA cycle
381	1.388	1.388	Malate dehydrogenase	EC:1.1.1.37	mal + nad ⟺ oaa + nadh + H	TCA cycle

See Additional file 2 for the FVA results of all 32 reactions involving NADH; Reaction ID and metabolite abbreviations are detailed in [70]

Table 11 The identified reactions that contribute significantly to the predicted maximum current output in the NADH-dependent mixotrophic mode

Reaction ID	NADH flux (mmol/gDW/h)		Enzyme	EC no.	Reaction	Subsystem
	Min	Max				
73	0	10.87	NAD(P) + transhydrogenase	EC:1.6.1.2	nadph + nad → nadp + nadh	Energy metabolism
106	−0.0011	10.87	Enoyl-ACP reductase	EC:1.3.1.9	dodecaACP + nad ⟺ tddec2eACP + nadh + H	Fatty acid biosynthesis
140	0.00249	2.723	D-3-phosphoglycerate dehydrogenase	EC:1.1.1.95	3 pg + nad ⟺ 3ppop + nadh + H	Glycine, serine, cysteine biosynthesis
251	−0.00111	10.87	Homoserine dehydrogenase	EC:1.1.1.3	hom-L + nad ⟺ aspsa + nadh + H	Methionine biosynthesis
288	0	2.720	Delta-1-pyrroline-5-carboxylate dehydrogenase	EC:1.5.1.12 1.5.99.8	1pyr5c + nad + 2 h2o → glu-L + nadh + H	Proline biosynthesis
171	−1.784	10.90	Glyceraldehyde-3-phosphate dehydrogenase	EC:1.2.1.59	gap + pi + nad ⟺ bpg + nadh + H	Glycolysis
NADH-consuming reactions						
134	−2.720	0	Glutamate synthase	EC:1.4.1.14	gln-L + akg + nadh + H → 2 glu-L + nad	Glutamate, glutamine biosynthesis
381	−2.718	0.0022	2-ketoacid dehydrogenase malate dehydrogenase lactate dehydrogenase	EC:1.1.1.37	mal + nad ⟺ oaa + nadh + H	TCA cycle

See Additional file 2 for the FVA results of all 32 reactions involving NADH; Reaction ID and metabolite abbreviations are detailed in [70]

result in an excess flux of up to 4.177 mmol/gDW/h. The major portion of the excess reduced-ferredoxin flux was balanced by ferredoxin-dependent glutamate synthase (EC: 1.4.7.1) and the remainder was consumed by sulfite reductase (EC: 1.8.7.1), to make up a net sum flux of 7.310 mmol/gDW/h. The present result confirms the previous notion that the ferredoxin-NADP oxidoreductase (EC: 1.18.1.2) is the electron supplying site to reduce the mediator, 2-hydroxy-1, 4-naph-thoquinone (HNQ), in the cyanobacteria-based MFC [67].

In addition, the other three ferredoxin-involved reactions had no flux under high current output. This may be attributed to a cellular mechanism that reallocates metabolic resource to those pathways that can regenerate ferredoxin more efficiently, while maximizing the biomass production rate. Compared with ferredoxin-NADP oxidoreductase, the three reactions with zero fluxes probably have lower efficiency or capability to regenerate reduced-ferredoxin flux to meet the heavy demand at high current output and are thus abandoned by the metabolism.

Plastoquinol (QH_2)-dependent photoautotrophic mode

Akin to the case of ferredoxin-linked MET, only one reaction (reaction ID 281) was identified as capable of regenerating plastoquinol at a high enough rate to sustain the theoretical maximum current production (Table 8). This reaction could solely supply about 105 % of the maximum net plastoquinol flux (13.92 mmol/gDW/h) towards mediator. Since the identified reaction takes place at a location of the photosystem II of the photosynthetic electron transport chain, the present result is consistent with previous reporting that the site between photosystem II reaction and Q_B (Quinone binding) protein is the main location supplying electrons for the exogenous mediator, HNQ, in a cyanobacteria-based MFC [57].

The 5 % surplus plastoquinol flux was consumed by another two reactions (ID 284 & 285) for producing NADPH and $FADH_2$. NADPH is used to provide energy for the Calvin–Benson cycle that produces other carbohydrates such as starch and sucrose, as required for biomass synthesis, whereas $FADH_2$ participates in generating a proton motive force that can drive the synthesis of ATP. This indicates that the plastoquinol-consuming reactions are important to the survival of the cell.

In the conventional paradigm, under normal growth of *Synechocystis* sp. PCC 6803, the plastoquinol pool can be replenished by three sources (Fig. 1): $FADH_2$, NAD(P)H, and photosynthesis light reactions [60], and the actual metabolic source for plastoquinol production during electricity generation is hard to identify. However, the FVA analysis result has elucidated that the plastoquinol available for the electrochemical reaction in MFCs is produced

from the photosynthesis light reaction, rather than from the other two sources, i.e., reactions catalyzed by NADH dehydrogenase (EC:1.6.99.3,1.6.5.3) or $FADH_2$ in the process of cyclic electron flow.

The discussion above proves that plastoquinol is a good candidate electron source to be targeted by mediators for the MET mode. Recently, it has been found that *Synechocystis* sp. PCC 6803 can perform DET in an MFC without the addition of mediators [72], and this cyanobacterium can also produce electrically conductive nanowires (nanopili) to facilitate the DET mode [3, 12]. The DET mode uses an electron transfer mechanism to deposit the electrons from the c-type cytochrome to the anode. As described in the "Materials and methods" section, this process was modeled by incorporating another two reactions in the network: one describes the electron transfer from plastoquinone to the cytochrome, and the other one captures the mechanism of the electron transfer from the cytochrome to anode, leaving the oxidized form of the protein complex inside the thylakoid membrane. It is found that modeling the availability of plastoquinol for MET is equivalent to modeling the c-type cytochrome-associated DET. Although this phenomenon is still in keeping with a previous idea that the DET mode of the *Synechocystis* is related to the plastoquinone pool in the electron transfer chain [41], it could also be interpreted that the lack of further detailed mechanisms and constraints regarding the DET mode makes this model unable to tell the difference between DET and MET mode, both of which are influenced by the plastoquinol regeneration capability of the cell.

NADH-dependent photoautotrophic mode

In the autotrophic mode (Table 9), the maximum net NADH flux is computed to be 3.849 mmol/gDW/h, resulting from a combination of six NADH-producing routes and two NADH-consuming reactions. Each of the four NADH-producing reactions, catalyzed by NAD(P) transhydrogenase (EC: 1.6.1.2), enoyl-ACP reductase (EC: 1.3.1.9), homoserine dehydrogenase (EC: 1.1.1.3), and glyceraldehyde-3-phosphate dehydrogenase (EC: 1.2.1.59), respectively, could solely contribute up to 200 % of the maximum net NADH flux. The other two NADH-producing reactions, D-3-phosphoglycerate dehydrogenase (EC: 1.1.1.95) and delta-1-pyrroline-5-carboxylate dehydrogenase (EC: 1.5.1.12 1.5.99.8), could supply up to about 101 % of the maximum net value. Any excess percentages of the NADH flux were mainly balanced by a combination of three consuming reactions, catalyzed by glyceraldehyde-3-phosphate dehydrogenase (EC: 1.2.1.59), 2-ketoacid dehydrogenase (EC: 1.1.1.37) and glutamate synthase (EC: 1.4.1.14), respectively.

NADH-dependent heterotrophic mode

Under heterotrophic growth, the maximum net NADH flux (8.605 mmol/gDW/h) was achieved through six reactions (Table 10). However, each reaction alone could only produce an NADH flux ranging from 16.13 to 51.50 % of the 8.605 mmol/gDW/h and thus these reactions had to work together to achieve the identified maximum net flux value. Notably, the fluxes associated with dihydrolipoamide dehydrogenase (EC: 1.8.1.4) and malate dehydrogenase (EC: 1.1.1.37) were inflexible, which indicates that the TCA cycle encompassing these two reactions is necessary to the glucose catabolism for sustaining biomass production. Furthermore, in contrast to the other two cultivation conditions (photoautotrophic and mixotrophic), there were no reactions that consumed NADH at a high rate (>1 mmol/gDW/h).

The reactions identified with potential for a high NADH regeneration rate are distributed in four conventional biological subsystems: energy metabolism, fatty acid biosynthesis, methionine biosynthesis, and glycolysis. It is found that the up-regulation of glycolysis was one of four ways to increase the NADH regeneration rate for *Synechocystis*, but not used by *G. sulfurreducens*, which employed strategies of overexpression of enzymes in the TCA cycle, amino acids and/or fatty acids pathways [30]. The involvement of glycolysis in the case of *Synechocystis* could be ascribed to the use of complex carbohydrate (i.e., glucose) as the substrate, which is different from the simple carbon source, acetate, chosen for the growth of *G. sulfurreducens*.

NADH-dependent mixotrophic mode

In the mixotrophic mode, the maximum net NADH flux (8.192 mmol/gDW/h) for MFC current production results mainly from the combined fluxes of eight reactions. Six of the eight reactions were used for NADH regeneration, whereas the other two reactions balanced any excess NADH fluxes of the production reactions. Among the six NADH-producing reactions, four reactions, $NAD(P)^+$ transhydrogenase (EC:1.6.1.2), enoyl-ACP reductase (EC:1.3.1.9) homoserine dehydrogenase (EC:1.1.1.3) and glyceraldehyde-3-phosphate dehydrogenase (EC:1.2.1.59), are the main routes selected by the cell to sustain the heavy NADH shunt during current production. Each of these four reactions could solely supply up to about 133 % of the maximum net NADH regeneration rate, which was four-fold higher than the other two lower potential reactions, catalyzed by D-3-phosphoglycerate dehydrogenase (EC: 1.1.1.95) and delta-1-pyrroline-5-carboxylate dehydrogenase (EC: 1.5.1.12; 1.5.99.8), each of which had a capability to achieve only up to 33 % of the maximum net NADH flux. The 33 % NADH excess was mainly

consumed by two reactions, glutamate synthase (EC: 1.4.1.14) and 2-ketoacid dehydrogenase/malate dehydrogenase/lactate dehydrogenase (EC: 1.1.1.37). Since these eight reactions were allowed to adjust their fluxes within certain ranges (Table 11), any combination of the fluxes of these NADH involved reactions that make up the maximum net NADH production rate is viable. This indicates that there are unlimited metabolic states (each corresponds to a functional phenotype) at which *Synechocystis* sp. PCC 6803 can sustain a high current output if the NADH serves as the electron supplier targeted in the MET mode.

Comparison of the metabolic strategies identified for the NADH-linked photoautotrophic, heterotrophic, and mixotrophic modes indicated that the electron supplying metabolic pathways activated in the three modes shared five reactions NAD(P) transhydrogenase (EC: 1.6.1.2), enoyl-ACP reductase (EC: 1.3.1.9), glyceraldehyde-3-phosphate dehydrogenase (EC: 1.2.1.59), homoserine dehydrogenase (EC: 1.1.1.3) and malate dehydrogenase (EC: 1.1.1.37). Only one reaction, dihydrolipoamide dehydrogenase (EC: 1.8.1.4), was used in the heterotrophic mode, but not in the other two modes. The mixotrophic and autotrophic growth employed the same set of reactions to regenerate NADH at a high rate. This is in accordance with the previous notion that the mixotrophic and photoautotrophic metabolic features are similar in *Synechocystis* sp. PCC6803 [56].

To elucidate how nutrient uptake is conveyed to biomass growth and current yield respectively, the following section compares the corresponding fluxes at different uptake rates.

Effect of varying glucose uptake and light uptake rates on predicted biomass and reducing equivalent production rates

The effect of varying substrate uptake rates on the biomass production or the electron transfer rates in all five current producing cases can be described using linear equations (Table 12). This suggests that substrate (i.e., either glucose or light) uptake rate is the major limiting factor for both biomass and current productivity.

Column 3 of Table 12 shows that the slopes of the linear regression equations for the biomass production rates were highly reduced compared to optimal growth, due to the severe reducing equivalent deprivation during electricity generation. Also, the slopes of the linear equations in column 4 are much higher than those of the equations in column 3. This indicates that the cell can produce all the three electron shuttles (i.e., ferredoxin, plastoquinol and NADH) much more efficiently than biomass.

Comparison of the slopes of the equations in column 3 also shows that the glucose rate has greater influence on the biomass and reducing equivalent production than light, since the slopes of plots of cumulative biomass produced

Table 12 The summary of linear functions of the biomass and the reducing equivalent production rates

	Metabolic type	Substrate	Growth (g/gDW/h)	Reducing equivalent production	
				(g/gDW/h)	(mmol/gDW/h)
Aerobic	Ferred &Photo	light	$y_c = 0.0026x$	$y_{(g/gDW/h)} = 0.4769x$	$y_{(mmol/gDW/h)} = 0.4747x$
			$y_p = 0.0002x$		
	QH2 &Photo	light	$y_c = 0.0026x$	$y_{(g/gDW/h)} = 0.782x$	$y_{(mmol/gDW/h)} = 0.9037x$
			$y_p = 0.0002x$		
	NADH &Photo	light	$y_c = 0.0026x$	$y_{(g/gDW/h)} = 0.162x$	$y_{(mmol/gDW/h)} = 0.2435x$
			$y_p = 8E\text{-}05x$		
	NADH & Hetero	glucose	$y_c = 0.1046x$	$y_{(g/gDW/h)} = 6.726x$	$y_{(mmol/gDW/h)} = 10.108x$
			$y_p = 0.0034x$		
	NADH & Mixo	light	$y_c = 0.0029x + 0.0446$	$y_{(g/gDW/h)} = 0.0.1769 + 2.788$	$y_{(mmol/gDW/h)} = 0.2658x + 4.1895$
			$y_p = 9E\text{-}05x + 0.0014$		
		glucose	$y_c = 0.1273x + 0.0393$	$y_{(g/gDW/h)} = 7.778x + 2.495$	$y_{(mmol/gDW/h)} = 11.689x + 3.7501$
			$y_p = 0.0039x + 0.0013$		

The FBA simulations were performed by changing the photon uptake rate and the glucose uptake rate with the maximization of the objectives. For the mixotrophic mode, the two separate sets of equations were obtained by (a) varying glucose uptake rate while the photon uptake rate was fixed to a value (as discussed in the "Materials and methods" section); (b) varying photon uptake rate while the glucose uptake rate was constrained to a given range. y denotes the reducing equivalent production rate for current generation (mmol/gDW/h or g/gDW/h) or growth rate (g/gDW/h), whereas x represents the substrate (i.e., glucose or light) uptake rates (mmol/gDW/h). y_c represents the optimal growth, whereas y_p denotes the perturbed growth under cytosolic NADH deprivation

versus glucose consumed were higher than those for the light. This could be attributed to the higher energy content in glucose than in light (8 electrons in each one glucose molecule, versus 2 electrons carried by each photon, as discussed in the "Materials and methods" section).

The efficiency of conversion of glucose to biomass in the mixotrophic (slope = 11.689) growth was higher than that in the heterotrophic (slope = 10.108) growth. And, the efficiency of the conversion of the photon to biomass in the mixotrophic (slope = 0.2658) growth was higher than that in the autotrophic (slope = 0.2435) growth. Thus, this indicates that the respiratory metabolism complements the photosynthesis in the mixotrophic growth. In other words, the respiratory and photosynthetic metabolisms are interconnected and form a synergetic relationship, due to the fact that the by-products of the photosynthetic reactions could be used as substrates for respiratory reactions and the simultaneous activation of the two energy metabolic pathways can improve the efficiencies of the reactions in each of the two pathways. Taken together, mixotrophic mode performs better in the conversion of the substrates to any of the three reducing equivalents than the photoautotrophic and heterotrophic modes.

By comparison of the line slopes for the three electron transfer cases of the photoautotrophic mode, higher substrate-to-product conversions (i.e., higher slopes of the lines) were seen with the plastoquinol than the other two electron sources, ferredoxin and NADH. This indicates that additional plastoquinol production is more favored for the *Synechocystis* compared with the other two electron sources, and thus it is a cost effective feedstock for current production.

Finally, the five operation modes are compared for their theoretically maximum current output in Fig. 4 and Table 13.

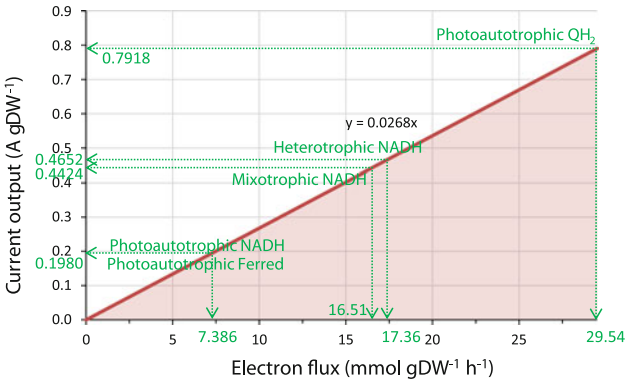

Fig. 4 The current output (A/g) as a function of electron flux. The *dark red line* denotes the maximal current outputs and reducing equivalent production rates, while the area represents all allowable current outputs and electron production rates. The *round dotted arrow line* indicates the maximal current output and corresponding electron production rate when the growth rate is set to 5 % of the predicted maximum growth rate (0.001967 h^{-1}) (color figure online)

Comparison of amperage outputs of the five electron transfer cases

Comparison of the results of five metabolic models for theoretically maximum current output (Fig. 4; Table 13) shows that the highest current output was 0.7918 A/gDW, which was achieved by using plastoquinol as the electron source under photoautotrophic growth. The metabolism of *Synechocystis* sp. PCC 6803 could recover the electrons from photon to plastoquinol at a coulombic efficiency of 95.91 %. When electricity generation was linked to NADH or reduced ferredoxin, the metabolism produced current at about 0.1980 A/gDW. The coulombic efficiencies for

Table 13 Comparison of predicted amperage outputs of five modes under theoretical maximum current output condition

Mode	Condition	Biomass production rate	Electron (mmol gDW^{-1} h^{-1})	Amperage (A gDW^{-1})	Coulombic efficiency (CE%)	W gDW^{-1}
Photoautotrophic Ferred	5% of optimal growth rate	0.001967	7.386	0.198	23.98%	0.184
Photoautotrophic QH2			29.54	0.7918	95.91%	0.325
Photoautotrophic cyt c						0.203
Photoautotrophic NADH			7.386	0.198	23.98%	0.164
Heterotrophic NADH			17.36	0.4652	85.09%	0.386
Mixotrophic NADH			16.51	0.4424	41.35%	0.367

Ferred reduced ferredoxin, *QH2* plastoquinol, *cyt c* c-type cytochrome

production of these two redox molecules were comparatively low, at 23.98 %, suggesting the light-driven metabolism is not efficient in either NADH or ferredoxin regeneration. When NADH was modeled as the electron source for electricity generation, similar levels of current outputs were obtained for mixotrophic (0.4424 A/gDW) and heterotrophic growth (0.4652 A/gDW). The slightly lower current output of the mixotrophic mode is due to a lower upper limit of glucose uptake rate (0.38 mmol/gDW/h) used in the simulations of mixotrophic growth, compared with a much higher upper bound of 0.85 mmol/gDW/h chosen for modeling heterotrophic growth. These two upper bounds for the two growth modes were experimentally determined in a previous study [68]. In addition, the coulombic efficiency was much lower for mixotrophic growth (41.35 %) than for heterotrophic growth (85.09 %). This is attributed to the smaller number of electrons liberated from each one photon than from one glucose molecule.

Although the plastoquinol and c-type cytochrome-dependent electricity generation produced much higher current than NADH-dependent modes, their power outputs were lower than the NADH-dependent counterparts due to lower formal potential of plastoquinol and c-type cytochrome. Nevertheless, this minor weakness should be outweighed by the other two advantages, i.e., much higher current productivity and the economic operation cost in the photoautotrophic growth, which does not need the organic carbon source. Taken together, these results indicate that plastoquinol-targeted MET or cytochrome complex targeted DET mode is the best electron transfer mode that should be exploited during practical electricity generation than the other three operational cases studied here.

In experiments, the MFC based on *Synechocystis* sp. PCC6803 could reach a maximum power density output of 6.7 of mW m^{-3} in the photoautotrophic growth mode, without addition of exogenous mediator [26]. The cell density in this MFC system was about 6×10^{9} cells/ml [26]. For estimation of the theoretical maximum power output in this previous study, an assumed dry weight of 2×10^{-13} g per cell [65], together with the measured cell density reported, can be used to convert the presently computed maximum power density for plastoquinol and c-type cytochrome targeted electricity generation into 308 and 192.58 W m^{-3}, respectively. These two values serve as the theoretical upper bounds of the DET mode outputs of the *Synechocystis* at the literature cell density (6×10^{9} cells/ml) aforementioned. These upper limits of the power densities are at least a thousand times greater than the practically reported ones. Some reasons for such a large discrepancy could be ascribed to the fact that in the calculation, we assume every single cell in a volume of m^3 lives in the optimal metabolic state and can contribute to the power generation to its maximum capability. In practice, only cells attached to the anode can participate in the DET current production and only part of the surface of the cells on the outsides of the culture can intercept light to conduct photosynthesis. Our results nevertheless suggest a large potential for improvement of current yields from currently obtained experimental values.

Comparison of the production capability of the three potential reducing equivalents (i.e., ferredoxin, plastoquinol and NADH) indicates that plastoquinol or plastoquinol-linked c-type cytochrome is the best electron source to be targeted for MFC current production. Previous study has found that the *Synechocystis* sp. PCC 6803 can conduct photosynthesis and respiration simultaneously, because its respiratory and photosynthetic electron transport pathways intersect in the thylakoid membrane and enzymes and electron carriers, such as cytochrome b_6f complex and plastoquinone pool, are shared between the electron transport chains [34, 60]. Therefore, the redox shuttle, plastoquinol or its successively linked cytochrome complex would be ideal for supplying electrons towards anode not only in the autotrophic mode, but also in heterotrophic or mixotrophic modes, in which the two electron flows through both photosynthesis and catabolism of a carbon source are added up.

However, current output based on the plastoquinol replenished by the electron transfer chains may have a disadvantage in that only one reaction can be targeted as the electron supplier. On the other hand, the results of the present study have shown that a high flux of NADH can be achieved by unlimited combinations of the fluxes of a number of NADH-involved reactions. This indicates that the metabolism is naturally optimized for NADH-dependent by-product synthesis and the NADH targeted current production can endure more environmental perturbations since many metabolic states (pathways) can produce the same high level of current. In addition, the relatively low (negative) redox potential of NADH is also another merit for selecting this currency metabolite as the terminal electron shuttle in MFC applications [49].

The metabolic flux model for the *Synechocystis* in the present study was computed based on a genome-scale network. This is different from many other studies that usually conduct modeling on the effective model of the metabolism of *Synechocystis*, considering only nearly 100 reactions [51]. Compared with such simplified networks, the genome-scale metabolic network contains essential and non-essential reactions and is more suitable for modeling microorganisms under extreme conditions such as a higher current generation in MFC conditions in which the non-essential reactions may become activated and consequently responsible for the optimization for the desired metabolite production.

Conclusions

The present study modeled five cases of MFC electricity generation based on *Synechocystis* sp. PCC6803. The analysis of the resultant flux models indicates that plastoquinol is the best electron source to be targeted to liberate the maximum capability of the cyanobacteria for current production, since the pertinent electrochemical reaction had a potential to supply a higher electron flux than the reactions based on the other two studied sources (reduced ferredoxin and NADH). The site with the highest potential for plastoquinol regeneration was confirmed to be the electron transfer chain reaction situated between the PSII and PSI complexes. Besides, the fractional benefit analysis has further implied the suitability of the plastoquinol/cytochromes targeted MET or DET modes for *Synechocystis* sp. PCC 6803.

Compared with autotrophic and heterotrophic conditions, the photosynthesis and oxidative phosphorylation of the mixotrophic metabolism could form a synergetic relationship, improving the efficiency of converting glucose and photons into NADH. Even though the current output in the simulations was slightly higher for heterotrophic than for mixotrophic growth, this was under the assumption of a much lower glucose uptake rate in the mixotrophic mode. This is a conservative assumption based on the observed uptakes rates in unperturbed growth. It is quite plausible that without this restriction, the glucose uptake rate will be increased when NADH is extracted under mixotrophic growth conditions, to a value that is closer to that shown by heterotrophic growth to be physiologically feasible. In that case, the mixotrophic current output would be considerably higher than those we calculated. The considerations above suggest that mixotrophic growth is more efficient and can yield a higher current output per unit substrate uptake rate, and consequently is an ideal nutritional condition for the cyanobacterium.

Future studies could employ the metabolic engineering strategies such as adaptive evolution, or rationally devised gene-knockout strategies, with the aid of knowledge of the metabolic pathways identified here, to practically achieve a higher current production for MFC using this biocatalyst.

References

1. Atsumi S, Higashide W, Liao JC (2009) Direct photosynthetic recycling of carbon dioxide to isobutyraldehyde. Nat Biotechnol 27(12):1177–1180. doi:10.1038/nbt.1586
2. Babanova S, Hubenova Y, Mitov M (2011) Influence of artificial mediators on yeast-based fuel cell performance. J Biosci Bioeng 112(4):379–387. doi:10.1016/j.jbiosc.2011.06.008
3. Bhaya D (2004) Light matters: phototaxis and signal transduction in unicellular cyanobacteria. Mol Microbiol 53(3):745–754. doi:10.1111/j.1365-2958.2004.04160.x
4. Boesen T, Nielsen LP (2013) Molecular dissection of bacterial nanowires. MBio 4(3). doi:10.1128/mBio.00270-13
5. Chang RL, Ghamsari L, Manichaikul A, Hom EFY, Balaji S, Fu W, Shen Y, Hao T, Palsson BO, Salehi-Ashtiani K, Papin JA (2011) Metabolic network reconstruction of Chlamydomonas offers insight into light-driven algal metabolism. Mol Syst Biol 7. URL http://www.nature.com/msb/journal/v7/n1/suppinfo/msb201152_S1.html
6. Cheetham NWH (2011) Introducing biological energetics: how energy and information control the living. World Oxford University Press, New York
7. Cheng S, Liu H, Logan BE (2006) Increased power generation in a continuous flow MFC with advective flow through the porous anode and reduced electrode spacing. Environ Sci Technol 40(7):2426–2432. doi:10.1021/es051652w
8. Du Z, Li H, Gu T (2007) A state of the art review on microbial fuel cells: a promising technology for wastewater treatment and bioenergy. Biotechnol Adv 25(5):464–482. doi:10.1016/j.biotechadv.2007.05.004
9. Dutta D, De D, Chaudhuri S, Bhattacharya SK (2005) Hydrogen production by Cyanobacteria. Microb Cell Fact 4:36. doi:10.1186/1475-2859-4-36
10. Ekins S, Honeycutt JD, Metz JT (2010) Evolving molecules using multi-objective optimization: applying to ADME/Tox. Drug Discov Today 15(11–12):451–460. doi:10.1016/j.drudis.2010.04.003
11. Feng X, Xu Y, Chen Y, Tang YJ (2012) Integrating flux balance analysis into kinetic models to decipher the dynamic metabolism of *Shewanella oneidensis* MR-1. PLoS Comput Biol 8(2):e1002376. doi:10.1371/journal.pcbi.1002376
12. Gorby YA, Yanina S, McLean JS, Rosso KM, Moyles D, Dohnalkova A, Beveridge TJ, Chang IS, Kim BH, Kim KS, Culley DE, Reed SB, Romine MF, Saffarini DA, Hill EA, Shi L, Elias DA, Kennedy DW, Pinchuk G, Watanabe K, Ishii S, Logan B, Nealson KH, Fredrickson JK (2006) Electrically conductive bacterial nanowires produced by Shewanella oneidensis strain MR-1 and other microorganisms. Proc Natl Acad Sci USA 103(30):11358–11363. doi:10.1073/pnas.0604517103
13. Gorby YA, Yanina S, McLean JS, Rosso KM, Moyles D, Dohnalkova A, Beveridge TJ, Chang IS, Kim BH, Kim KS, Culley DE, Reed SB, Romine MF, Saffarini DA, Hill EA, Shi L, Elias DA, Kennedy DW, Pinchuk G, Watanabe K, Ishii SÄ, Logan B, Nealson KH, Fredrickson JK (2006) Electrically conductive bacterial nanowires produced by Shewanella oneidensis strain MR-1 and other microorganisms. Proc Natl Acad Sci 103(30):11358–11363. doi:10.1073/pnas.0604517103
14. Johnson CH, Stewart PL, Egli M (2011) The cyanobacterial circadian system: from biophysics to bioevolution. Annu Rev Biophys 40:143–167. doi:10.1146/annurev-biophys-042910-155317
15. Kaneko T, Sato S, Kotani H, Tanaka A, Asamizu E, Nakamura Y, Miyajima N, Hirosawa M, Sugiura M, Sasamoto S, Kimura T, Hosouchi T, Matsuno A, Muraki A, Nakazaki N, Naruo K, Okumura S, Shimpo S, Takeuchi C, Wada T, Watanabe A, Yamada M, Yasuda M, Tabata S (1996) Sequence analysis of the genome of the unicellular cyanobacterium *Synechocystis* sp. Strain PCC6803. II. Sequence determination of the entire genome and assignment of potential protein-coding regions. DNA Res 3(3):109–136. doi:10.1093/dnares/3.3.109
16. Kim BH, Park HS, Kim HJ, Kim GT, Chang IS, Lee J, Phung NT (2004) Enrichment of microbial community generating electricity using a fuel-cell-type electrochemical cell. Appl Microbiol Biotechnol 63(6):672–681. doi:10.1007/s00253-003-1412-6
17. Kim K-Y, Chae K-J, Choi M-J, Ajayi FF, Jang A, Kim C-W, Kim IS (2011) Enhanced coulombic efficiency in glucose-fed microbial fuel cells by reducing metabolite electron losses using dual-

anode electrodes. Bioresour Technol 102(5):4144–4149. doi:10.1016/j.biortech.2010.12.036
18. Kim N, Choi Y, Jung S, Kim S (2000) Development of microbial fuel cells using proteus vulgaris. Bull Korean Chem Soc 21(1):44–48
19. Kruk J, Jemioła-Rzemińska M, Strzałka K (2003) Cytochrome c is reduced mainly by plastoquinol and not by superoxide in thylakoid membranes at low and medium light intensities: its specific interaction with thylakoid membrane lipids. Biochem J 375(1):215–220. doi:10.1042/bj20021820
20. Kruse O, Rupprecht J, Mussgnug JH, Dismukes GC, Hankamer B (2005) Photosynthesis: a blueprint for solar energy capture and biohydrogen production technologies. Photochem Photobiol Sci 4(12):957–970. doi:10.1039/b506923h
21. Lawrence BA, Suarez C, DePina A, Click E, Kolodny NH, Allen MM (1998) Two internal pools of soluble polyphosphate in the cyanobacterium *Synechocystis* sp. strain PCC 6308: an in vivo 31P NMR spectroscopic study. Arch Microbiol 169(3):195–200. doi:10.1007/s002030050560
22. Loferer-Krossbacher M, Klima J, Psenner R (1998) Determination of bacterial cell dry mass by transmission electron microscopy and densitometric image analysis. Appl Environ Microbiol 64(2):688–694
23. Logan BE (2009) Exoelectrogenic bacteria that power microbial fuel cells. Nat Rev Microbiol 7(5):375–381
24. Logan BE, Hamelers B, Rozendal R, Schröder U, Keller J, Freguia S, Aelterman P, Verstraete W, Rabaey K (2006) Microbial fuel cells: methodology and technology. Environ Sci Technol 40(17):5181–5192
25. Lovley DR (2008) The microbe electric: conversion of organic matter to electricity. Curr Opin Biotechnol 19(6):564–571. doi:10.1016/j.copbio.2008.10.005
26. Madiraju KS, Lyew D, Kok R, Raghavan V (2012) Carbon neutral electricity production by *Synechocystis* sp. PCC6803 in a microbial fuel cell. Bioresour Technol 110:214–218. doi:10.1016/j.biortech.2012.01.065
27. Mahadevan R, Schilling CH (2003) The effects of alternate optimal solutions in constraint-based genome-scale metabolic models. Metab Eng 5(4):264–276. doi:10.1016/j.ymben.2003.09.002
28. Mao L, Verwoerd W (2013) Selection of organisms for systems biology study of microbial electricity generation: a review. Int J Energy Environ Eng 4(1):17. doi:10.1186/2251-6832-4-17
29. Mao L, Verwoerd WS Computational comparison of mediated MFC current generation capacity of Chlamydomonas reinhardtii in photosynthetic and respiratory growth modes (submitted)
30. Mao L, Verwoerd WS (2013) Model-driven elucidation of the inherent capacity of *Geobacter sulfurreducens* for electricity generation. J Biol Eng 7(1):14. doi:10.1186/1754-1611-7-14
31. McCormick AJ, Bombelli P, Scott AM, Philips AJ, Smith AG, Fisher AC, Howe CJ (2011) Photosynthetic biofilms in pure culture harness solar energy in a mediatorless bio-photovoltaic cell (BPV) system. Energy Environ Sci 4(11):4699–4709
32. McKinlay JB, Zeikus JG (2004) Extracellular iron reduction is mediated in part by neutral red and hydrogenase in *Escherichia coli*. Appl Environ Microbiol 70(6):3467–3474. doi:10.1128/AEM.70.6.3467-3474.2004
33. Nakamura Y, Kaneko T, Hirosawa M, Miyajima N, Tabata S (1998) CyanoBase, a www database containing the complete nucleotide sequence of the genome of *Synechocystis* sp. strain PCC6803. Nucleic Acids Res 26(1):63–67. doi:10.1093/nar/26.1.63
34. Navarro E, Montagud A, Fernández de Córdoba P, Urchueguía JF (2009) Metabolic flux analysis of the hydrogen production potential in *Synechocystis* sp. PCC6803. Int J Hydrogen Energy 34(21):8828–8838. doi:10.1016/j.ijhydene.2009.08.036
35. Okamoto A, Nakamura R, Hashimoto K (2011) In-vivo identification of direct electron transfer from Shewanella oneidensis MR-1 to electrodes via outer-membrane OmcA–MtrCAB protein complexes. Electrochim Acta 56(16):5526–5531. doi:10.1016/j.electacta.2011.03.076
36. Orth JD, Thiele I, Palsson BO (2010) What is flux balance analysis? Nat Biotechnol 28(3):245–248. URL http://www.nature.com/nbt/journal/v28/n3/abs/nbt.1614.html#supplementary-information
37. Park DH, Kim SK, Shin IH, Jeong YJ (2000) Electricity production in biofuel cell using modified graphite electrode with Neutral Red. Biotechnol Lett 22(16):1301–1304. doi:10.1023/a:1005674107841
38. Park DH, Zeikus JG (2000) Electricity generation in microbial fuel cells using neutral red as an electronophore. Appl Environ Microbiol 66(4):1292–1297. doi:10.1128/aem.66.4.1292-1297.2000
39. Pereyra V, Saunders M, Castillo J (2013) Equispaced Pareto front construction for constrained bi-objective optimization. Math Comput Model 57(9–10):2122–2131. doi:10.1016/j.mcm.2010.12.044
40. Pinchuk GE, Hill EA, Geydebrekht OV, De Ingeniis J, Zhang X, Osterman A, Scott JH, Reed SB, Romine MF, Konopka AE, Beliaev AS, Fredrickson JK, Reed JL (2010) Constraint-based model of Shewanella oneidensis MR-1 metabolism: a tool for data analysis and hypothesis generation. PLoS Comput Biol 6(6):e1000822. doi:10.1371/journal.pcbi.1000822
41. Pisciotta JM, Zou Y, Baskakov IV (2010) Light-dependent electrogenic activity of cyanobacteria. PLoS ONE 5(5):e10821. doi:10.1371/journal.pone.0010821
42. Pisciotta JM, Zou Y, Baskakov IV (2011) Role of the photosynthetic electron transfer chain in electrogenic activity of cyanobacteria. Appl Microbiol Biotechnol 91(2):377–385. doi:10.1007/s00253-011-3239-x
43. Rabaey K, Verstraete W (2005) Microbial fuel cells: novel biotechnology for energy generation. Trends Biotechnol 23(6):291–298. doi:10.1016/j.tibtech.2005.04.008
44. Reguera G, McCarthy KD, Mehta T, Nicoll JS, Tuominen MT, Lovley DR (2005) Extracellular electron transfer via microbial nanowires. Nature 435(7045):1098–1101. doi:10.1038/nature03661
45. Reguera G, Nevin KP, Nicoll JS, Covalla SF, Woodard TL, Lovley DR (2006) Biofilm and nanowire production leads to increased current in Geobacter sulfurreducens fuel cells. Appl Environ Microbiol 72(11):7345–7348. doi:10.1128/AEM.01444-06
46. Rocha I, Maia P, Evangelista P, Vilaca P, Soares S, Pinto JP, Nielsen J, Patil KR, Ferreira EC, Rocha M (2010) OptFlux: an open-source software platform for in silico metabolic engineering. BMC Syst Biol 4:45. doi:10.1186/1752-0509-4-45
47. Rosenbaum M, Schröder U (2010) Photomicrobial solar and fuel cells. Electroanalysis 22(7–8):844–855. doi:10.1002/elan.200800005
48. Schellenberger J, Que R, Fleming RM, Thiele I, Orth JD, Feist AM, Zielinski DC, Bordbar A, Lewis NE, Rahmanian S, Kang J, Hyduke DR, Palsson BO (2011) Quantitative prediction of cellular metabolism with constraint-based models: the COBRA Toolbox v2.0. Nat Protoc 6(9):1290–1307. doi:10.1038/nprot.2011.308
49. Schröder U (2007) Anodic electron transfer mechanisms in microbial fuel cells and their energy efficiency. Phys Chem Chem Phys 9(21):2619–2629
50. Sharma V, Kundu PP (2010) Biocatalysts in microbial fuel cells. Enzyme Microb Technol 47(5):179–188. doi:10.1016/j.enzmictec.2010.07.001
51. Shastri AA, Morgan JA (2005) Flux balance analysis of photoautotrophic metabolism. Biotechnol Prog 21(6):1617–1626. doi:10.1021/bp050246d
52. Shukla AK, Suresh P, Berchmans S, Rajendran A (2004) Biological fuel cells and their applications. Curr Sci 87(4):455–468

53. Song H-S, Ramkrishna D, Pinchuk GE, Beliaev AS, Konopka AE, Fredrickson JK (2013) Dynamic modeling of aerobic growth of Shewanella oneidensis. Predicting triauxic growth, flux distributions, and energy requirement for growth. Metab Eng 15(0):25–33. doi:10.1016/j.ymben.2012.08.004
54. Steuer R, Knoop H, Machné R (2012) Modelling cyanobacteria: from metabolism to integrative models of phototrophic growth. J Exp Bot 63(6):2259–2274. doi:10.1093/jxb/ers018
55. Sund CJ, McMasters S, Crittenden SR, Harrell LE, Sumner JJ (2007) Effect of electron mediators on current generation and fermentation in a microbial fuel cell. Appl Microbiol Biotechnol 76(3):561–568. doi:10.1007/s00253-007-1038-1
56. Takahashi H, Uchimiya H, Hihara Y (2008) Difference in metabolite levels between photoautotrophic and photomixotrophic cultures of *Synechocystis* sp. PCC 6803 examined by capillary electrophoresis electrospray ionization mass spectrometry. J Exp Bot 59(11):3009–3018. doi:10.1093/jxb/ern157
57. Tanaka K, Kashiwagi N, Ogawa T (1988) Effects of light on the electrical output of bioelectrochemical fuel-cells containing Anabaena variabilis M-2: mechanism of the post-illumination burst. J Chem Technol Biotechnol 42(3):235–240. doi:10.1002/jctb.280420307
58. van Hoek M, Merks R (2012) Redox balance is key to explaining full vs. partial switching to low-yield metabolism. BMC Syst Biol 6(1):22
59. Varma A, Palsson BO (1994) Metabolic flux balancing: basic concepts, scientific and practical use. Nat Biotechnol 12(10):994–998
60. Vermaas WFJ (2001) Photosynthesis and respiration in cyanobacteria. In: eLS. Wiley, London. doi:10.1038/npg.els.0001670
61. Verwoerd W (2011) A new computational method to split large biochemical networks into coherent subnets. BMC Syst Biol 5(1):25
62. Verwoerd W (2012) Interactive extraction of metabolic subnets—the Netsplitter software implementation. J Mol Eng Syst Biol 1(1):2–2
63. Virdis B, Freguia S, Rozendal RA, Rabaey K, Yuan Z, Keller J (2011) 4.18—microbial fuel cells. In: Editor-in-Chief: Peter W (ed) Treatise on water science. Elsevier, Oxford, pp 641–665. doi:10.1016/b978-0-444-53199-5.00098-1
64. Wang K, Liu Y, Chen S (2011) Improved microbial electrocatalysis with neutral red immobilized electrode. J Power Sour 196(1):164–168. doi:10.1016/j.jpowsour.2010.06.056
65. Whitman WB, Coleman DC, Wiebe WJ (1998) Prokaryotes: the unseen majority. Proc Natl Acad Sci 95(12):6578–6583
66. Wilkinson S (2000) "Gastrobots"—benefits and challenges of microbial fuel cells in foodpowered robot applications. Auton Robots 9(2):99–111. doi:10.1023/a:1008984516499
67. Yagishita T, Horigome T, Tanaka K (1993) Effects of light, CO2 and inhibitors on the current output of biofuel cells containing the photosynthetic organism *Synechococcus* sp. J Chem Technol Biotechnol 56(4):393–399. doi:10.1002/jctb.280560411
68. Yang C, Hua Q, Shimizu K (2002) Metabolic flux analysis in *Synechocystis* using isotope distribution from 13C-labeled glucose. Metab Eng 4(3):202–216. doi:10.1006/mben.2002.0226
69. Yang Y, Xu M, Guo J, Sun G (2012) Bacterial extracellular electron transfer in bioelectrochemical systems. Process Biochem 47(12):1707–1714. doi:10.1016/j.procbio.2012.07.032
70. Yoshikawa K, Kojima Y, Nakajima T, Furusawa C, Hirasawa T, Shimizu H (2011) Reconstruction and verification of a genome-scale metabolic model for *Synechocystis* sp. PCC6803. Appl Microbiol Biotechnol 92 (2):347–358. doi:10.1007/s00253-011-3559-x
71. Zhao F, Harnisch F, Schröder U, Scholz F, Bogdanoff P, Herrmann I (2006) Challenges and constraints of using oxygen cathodes in microbial fuel cells. Environ Sci Technol 40(17):5193–5199. doi:10.1021/es060332p
72. Zou Y, Pisciotta J, Billmyre RB, Baskakov IV (2009) Photosynthetic microbial fuel cells with positive light response. Biotechnol Bioeng 104(5):939–946. doi:10.1002/bit.22466